

PAPER • OPEN ACCESS

Ultrafast dynamics of exciton–polariton in optically tailored potential landscapes at room temperature

To cite this article: Fei Chen *et al* 2022 *J. Phys.: Condens. Matter* **34** 024001

View the [article online](#) for updates and enhancements.

You may also like

- [Exciton-polariton trapping and potential landscape engineering](#)
C Schneider, K Winkler, M D Fraser *et al.*
- [The Strongest Magnetic Fields on the Coolest Brown Dwarfs](#)
Melodie M. Kao, Gregg Hallinan, J. Sebastian Pineda *et al.*
- [FDTD and transfer matrix methods for evaluating the performance of photonic crystal based microcavities for exciton-polaritons](#)
Yi-Cheng Liu and Tim Byrnes







IOP | ebooks™

Bringing together innovative digital publishing with leading authors from the global scientific community.

Start exploring the collection—download the first chapter of every title for free.

Ultrafast dynamics of exciton–polariton in optically tailored potential landscapes at room temperature

Fei Chen¹, Hui Li^{1,*}, Hang Zhou², Ziyu Ye¹, Song Luo², Zheng Sun¹, Fenghao Sun¹, Jiawei Wang¹, Huailiang Xu¹, Hongxing Xu¹, Zhanghai Chen^{2,*} and Jian Wu^{1,3,4,*}

¹ State Key Laboratory of Precision Spectroscopy, East China Normal University, Shanghai 200241, People's Republic of China

² Department of Physics, College of Physical Science and Technology, Xiamen University, 361005 Xiamen, People's Republic of China

³ Collaborative Innovation Center of Extreme Optics, Shanxi University, Taiyuan, Shanxi 030006, People's Republic of China

⁴ CAS Center for Excellence in Ultra-intense Laser Science, Shanghai 201800, People's Republic of China

E-mail: hli@lps.ecnu.edu.cn, zhanghai@xmu.edu.cn and jwu@phy.ecnu.edu.cn

Received 9 August 2021, revised 2 October 2021

Accepted for publication 6 October 2021

Published 28 October 2021



CrossMark

Abstract

In this work, by using femtosecond angle-resolved spectroscopic imaging technique, the ultrafast dynamics of confined exciton–polaritons in an optical induced potential well based on a ZnO whispering-gallery microcavity is explicitly visualized. The sub-picosecond transition between succeeding quantum harmonic oscillator states can be experimentally distinguished. The landscape of the potential well can be modified by the pump power, the spatial distance and the time delay of the two input laser pulses. Clarifying the underlying mechanism of the polariton harmonic oscillator is interesting for the applications of polariton-based optoelectronic devices and quantum information processing.

Keywords: exciton polariton, ultrafast dynamics, confined quantum state, femtosecond angle-resolved photoluminescence spectroscopy


(Some figures may appear in colour only in the online journal)

1. Introduction

Exciton–polaritons (EPs) formed by strong coupling between confined photonic modes with excitons in semiconductor microcavities are bosonic quasiparticles which possess light and matter hybrid properties [1, 2]. EPs inherit from their photonic component fast operation speed and extremely light effective mass. The former makes EPs promising for the

realization of ultrafast signal processing, while the latter can lead to Bose–Einstein condensation at high (room) temperature where the particles can accumulate in the same quantum state when a threshold density is reached [3–6]. Condensation of EPs has been realized in a two-dimensional (2D) quantum well at cryogenic temperature in the year of 2006 [7]. With the high propagation speed and spatial-temporal coherence, EPs are regarded as promising candidate for building ultrafast signal processing devices [8–10]. Typically, the propagation and transition of polaritons take place at femtosecond to picosecond time scales, corresponding to terahertz (THz) operation speed in potential applications. Thus it is of great importance to explore the fundamental properties and interaction mechanism

* Authors to whom any correspondence should be addressed.

 Original content from this work may be used under the terms of the [Creative Commons Attribution 4.0 licence](https://creativecommons.org/licenses/by/4.0/). Any further distribution of this work must maintain attribution to the author(s) and the title of the work, journal citation and DOI.

of EPs, as well as to pursue effective means of controlling the EP dynamics.

For practical applications, the room-temperature operation turns to be an advantageous factor. The widely studied microcavity systems of distinct dimensionalities that hold stable EPs are mostly operated at cryogenic temperatures [11–13]. The temperature dependent dynamics indicate that polariton lifetime is decreasing at higher temperature [14]. Due to the large exciton binding energy and strong oscillator strength, the ZnO-based system can hold stable polaritons at room temperature. Moreover, the ZnO microwire grown by the chemical vapor deposition (CVD) method exhibits hexagonal cross-sections, which become naturally whispering gallery (WG) microcavities. The confined photons can be strongly coupled to semiconductor excitons in a high quality WG cavity to form long-lived polaritonic states. On the other hand, exciton polaritons in the ZnO microwire can mainly move along the long axis of the wire, making the system performing like a 1D system. In such systems, more efficient tailoring on polariton dynamics can be realized. In fact, cavity polaritons have been realized in ZnO WG microcavity a decade ago [15] and illuminated a lot of following works regarding, e.g. polariton parametric scatterings [16, 17] and external manipulations using tailored laser fields [18–25]. However, most of the research on room-temperature EPs in ZnO WG microcavity are carried out via static state measurements. Nevertheless, experimental spectroscopic data obtained in static conditions do not fully provide unambiguous evidence on the underlying mechanism. The complex coupling dynamics of EPs usually exhibit entangled processes between multiple degrees of freedom, thus a simultaneous detection of the energy and momentum information is required. Interference measurements that provide sub-picosecond (sub-ps) resolved spatial coherence information are widely used in the field. However, the transient energy and momentum dynamics cannot be detected simultaneously along with the scan [26]. To reveal the coherent nature of room-temperature EPs, advanced experimental techniques with the sub-ps resolution are highly desirable.

In the present work, femtosecond-resolved measurements on the coupling dynamics of cavity polaritons in ZnO WG microcavity are realized in both energy and momentum degrees of freedom. Utilizing optically-controlled potentials, polariton harmonic oscillators are tailored with high precisions in both space and time. This prototype system can serve as a building block for further complex polariton structures. Our work paves the way for the applications of advanced polariton devices for all-optical manipulation.

2. Experimental materials and methods

The sample we used are ZnO microwires grown along the c -axis by the CVD method. The high quality factor of the WG microcavity is formed naturally by the inherent structure with a hexagonal cross-section. The diameters of microwires are in the range of 2–4 μm and the length exceeds 100 μm . The ZnO-based microcavity shows great advantage for room temperature operation due to its wide bandgap (about 3.3 eV), the large exciton binding energy (around 60 meV) and the

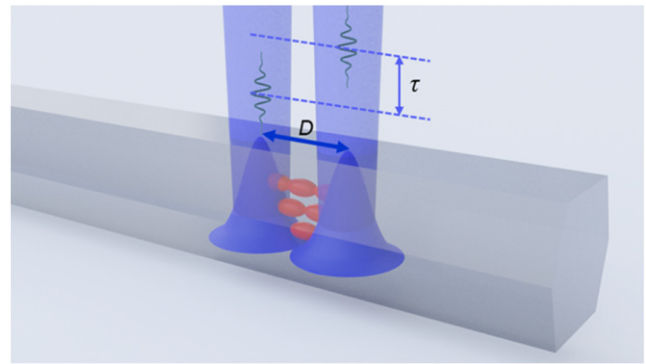


Figure 1. Schematics of the parabolic potential well generated by two laser beams. Exciton polaritons trapped in the potential well form new quantum states.

strong oscillator strength. The excitation pulses are synchronized femtosecond pulses at the central wavelength of 350 nm at the repetition rate of 1 kHz which are produced through an optical parametric amplifier (TOPAS). The pulse duration is about 240 fs (FWHM). The polariton condensate is excited non-resonantly by a pair of focused femtosecond pulses (with spot size about 3 μm in diameter) at separations of a few microns. The spatial separated optical excitation can provide symmetric or asymmetric transient parabolic trap profile and the width of the potential wells can be tuned by the separation between the two laser beams. Strong coupling of cavity polariton wave packets can be initiated, forming polariton harmonic oscillators (schematically shown in figure 1).

The angle-resolved photoluminescence (PL) spectroscopy measurement is performed by using a spectrometer (with the focal length of 500 mm and the grating specific as 1200 g mm^{-1}) with a 2D intensified charge-coupled device. Particularly, the femtosecond angle-resolved spectroscopic imaging (FARSI) technique is implemented to visualize the dynamics of polariton evolution [17, 27, 28] in both energy and momentum degrees of freedom with good signal-to-noise ratios. The optical Kerr gating is controlled by a beam of 35 fs femtosecond pulses at 800 nm with pulse energies of about 300 μJ . The time resolution, which is determined by the parameters of the pumping pulses, the precision of the delay line, and the properties of the Kerr media, etc, is estimated to be around 35 fs.

3. Dynamics of polariton condensates in tailored potential wells

3.1. Dynamics of polariton condensates in potential wells with controlled width

In this section, potential wells with controlled widths are realized by changing the spatial separation between two laser beams. Polariton harmonic oscillators with various highest excited SHO (simple harmonic oscillator) states characterized by different node numbers are obtained. In the non-resonant excitation regime, exciton reservoir is firstly generated by femtosecond injection, which undergoes effective cooling [29].

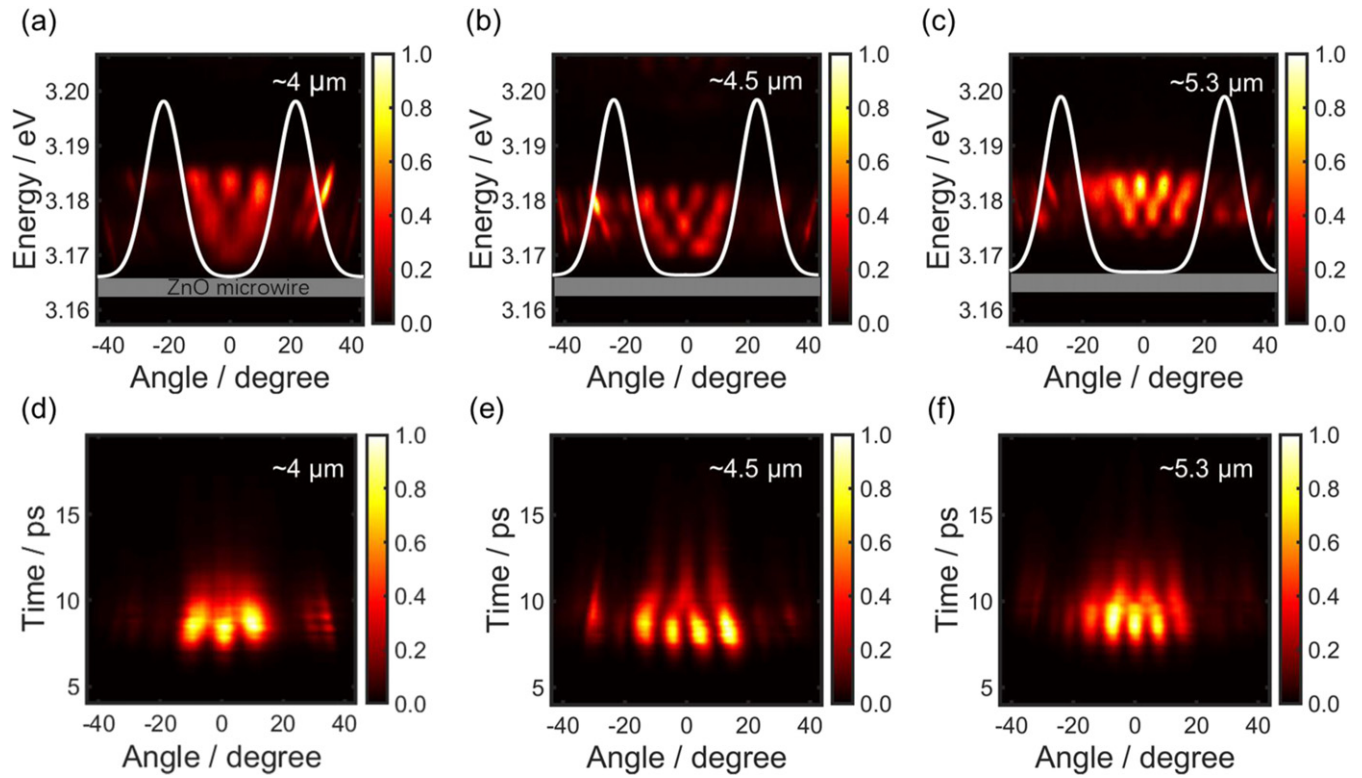


Figure 2. The static PL distributions and the dynamics of polariton condensates in width controlled potential wells. (a)–(c) The static angle-resolved PL images for different separations of the two laser beams. The separations are 4, 4.5, 5.3 micron, respectively. The white lines represent the landscape of the potential wells in real space. (d)–(f) Corresponding PL distributions as a function of emission angle and time for different separations.

The two exciton reservoirs perform essentially as two time-dependent potential barriers for polaritons. Polaritons sliding down to the potential well reform new quantum state. The time-integrated PL images at three distinct separations of the two laser beams are shown in figures 2(a)–(c). As the two laser beams leaving further apart, the number of nodes of the highest constrained quantum states is increased. By tuning the separation with sub-micron precision, we can obtain the uppermost quantum state of the harmonic oscillator with $n_{\text{SHO}} = 3, 4, \text{ and } 5$, corresponding to beam separations at 4.0, 4.5, and 5.3 μm , respectively. The energy spacing between the adjacent quantum states does decrease with the trap width increasing (energy level spacing is 6.2 meV, 4.5 meV and 4.0 meV). This phenomenon has been demonstrated in early work [20]. Here we reveal the underlying dynamics which was absent in former investigations. In the time-resolved angular distributions, the process of combination and redistribution of the polariton wave packets have been clearly observed, as shown in figures 2(d)–(f).

3.2. Dynamics of polariton condensates in symmetric/asymmetric potential wells

In this section, the harmonic/anharmonic oscillator constrained in symmetric/asymmetric potential well can be well manipulated by the light field strengths of the two excitation beams. We record the spatiotemporal oscillator dynamics formed in optically confined polariton condensates.

The typical angle-resolved PL images of polaritonic harmonic oscillators are shown in figures 3(a) and (d). When we use two laser beams with the same power to excite the ZnO microwire, symmetric harmonic potential can be formed thus the resulting polariton condensates will be confined within such potential well and follow the dynamics resembling a harmonic oscillator. Here, the strength of each excitation beam is tuned to be slightly beyond the condensation threshold ($P_{\text{th}} = 450 \text{ nW}$). The static (top) and transient (middle and bottom) angle-resolved PL images are presented in figure 3(a). In the time-integrated image, the interference pattern for a series of excited constrain states of $n_{\text{SHO}} = 10$ (node number) to the ground state can be recognized with equal energy spacing (around 2.2 meV), indicating the occupation of quantum harmonic oscillator states. The relative signal strength for the states with different quantum numbers show an energy-dependence. Based on the FARS technique, the dynamics showing how a quantum harmonic oscillator is formed can be explicitly visualized. Two distinct transient 2D images are shown in figure 3(a) (middle and bottom), presenting pure interference stripes formed by occupying two excited states observed at times of 7.11 ps and 8.31 ps, respectively. The momentum distributions of the instantaneous interference stripes can be well-reproduced using the quantum harmonic oscillator model [19] which are presented by the white dashed curves in figure 3(a). After the ultrafast injection, polaritons prefer to occupy a highly excited state initially and monotonically moves towards lower energies and smaller transverse

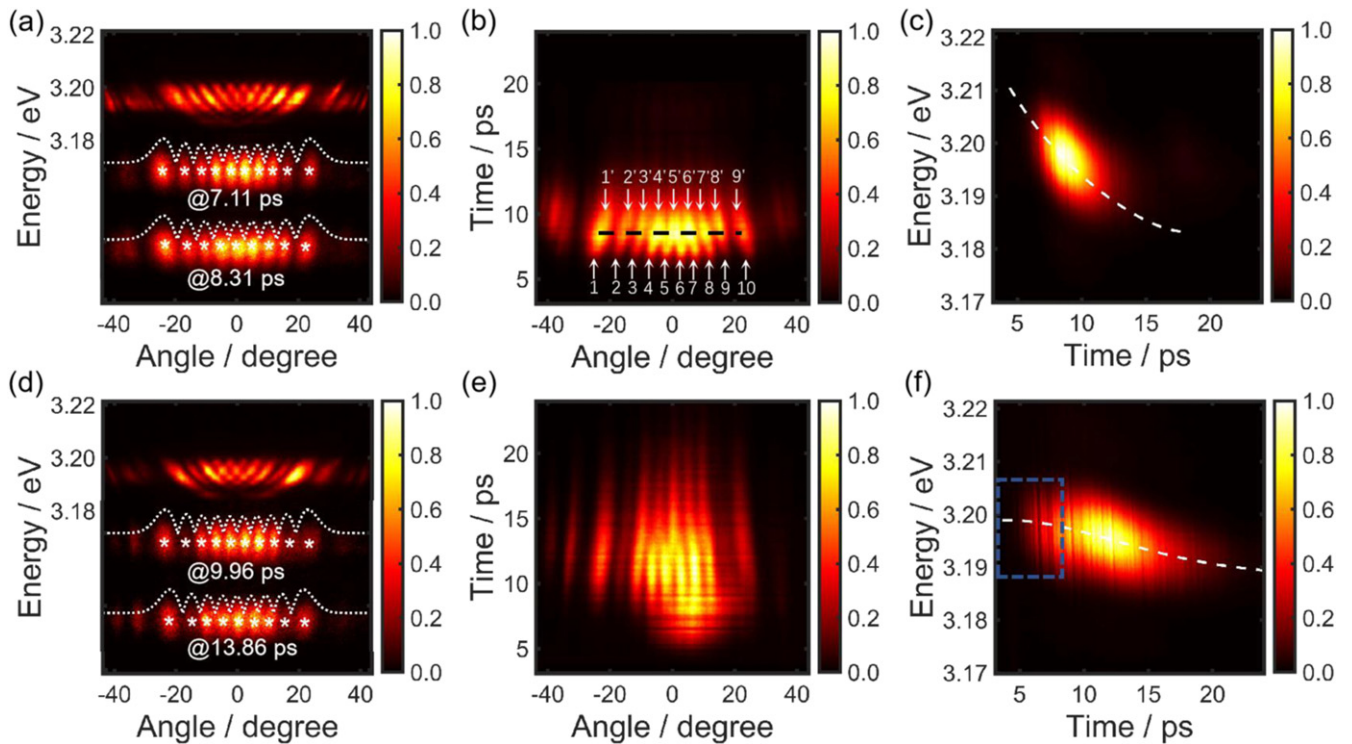


Figure 3. The static and femtosecond-resolved harmonic/anharmonic oscillator in the symmetric/asymmetric potential wells. (a) The static and selected transient (at indicated delays) angle-resolved PL images of the optically confined polaritons which are excited by two pulse lasers of the same power. White dashed lines are the fitting results by using the quantum harmonic oscillator model. (b) PL distributions as a function of emission angle and time in the momentum space. (c) Time-dependent PL distribution in the energy degree of freedom. The dashed curve helps to guide the eyes to see the redshift. (d)–(f) Similar to those of (a)–(c) but are obtained under anharmonic excitation condition with two uneven pumping power. The higher power of pump is on the right-hand side. The red shift exhibits an extra slow region at the beginning from 4.5 ps to 9.1 ps, indicated by the dashed rectangular in (f).

momenta. In our measurement, we can see that polaritons with $n_{\text{SHO}} = 10$ transit to the state with $n_{\text{SHO}} = 9$. Such process will keep on going until the lowest state with $n_{\text{SHO}} = 1$ is occupied. The polariton wavefunction at the highest confined state has the most significant overlap with the reservoir, therefore exhibit the highest gain [30]. The wave packet only has a small overlap for lower energy states leads to weaker emissions. Indeed, the polaritons can transfer from the top to the bottom of the cascade sequentially passing all the energy levels, this is the progress of bosonic cascade relaxation, where stimulated transitions occur in a ladder of equidistant energy levels [31]. Clearer transitions between more cascading states can be seen in figure 5(a). In addition, the depth of the potential well can be tailored by the optical field strength. If the power density of two laser beams are increased evenly, the depth of the potential well will increase, and the higher excited SHO state featured by larger node numbers will appear.

The time-resolved angular distribution of the PL emission in the momentum space is shown in figure 3(b). Initially, polaritons populate preferentially on the uppermost confined energy state with $n_{\text{SHO}} = 10$. The distribution undergoes a shrinking in the emission angle with a transition from $n_{\text{SHO}} = 10$ to $n_{\text{SHO}} = 9$ occurring at $t = 8.5$ ps (see the black dash line in figure 3(b)). In figure 3(b), it can be distinguished that the nodes marked by 1–10 populated at different emission angles transit to the nodes 1'–9', where the node 4' is formed

by combining part of the neighbouring nodes of 4 and 5 of the higher state, and etc. The transition takes place within 2 ps for the two adjacent quantum states. However, at the angle range of >10 degree, the nodes move to a relatively small angle as time going. The general tendency turned to be that the nodes at high state preferentially combine and generate a new one at the low state with small emission angles, while polariton nodes initially formed in larger angles shift towards smaller angles.

The energy redistribution among polaritons after femtosecond pulse excitation leads to a time-dependent red shift in the emission energy, which can be traced in our measurement and is shown in figure 3(c). Here the time-resolved PL images are integrated for all the emission angles at each time instant. A faster red shift can be recognized in the early stage which can be attributed to the stronger interactions among a larger population of polaritons at the beginning of the ejection. Then the redshift is slowed down due to the decreasing of polariton density since polaritons are decayed with lifetimes of a few picoseconds. There is no further supplement after the end of the femtosecond pumping pulse.

By simply tuning the relative intensity of the two excitation beams, an asymmetric optical potential can be formed and the constrained polaritons undergo anharmonic oscillations. The corresponding results for the polariton anharmonic oscillators are shown in figures 3(d)–(f). There is no apparent difference

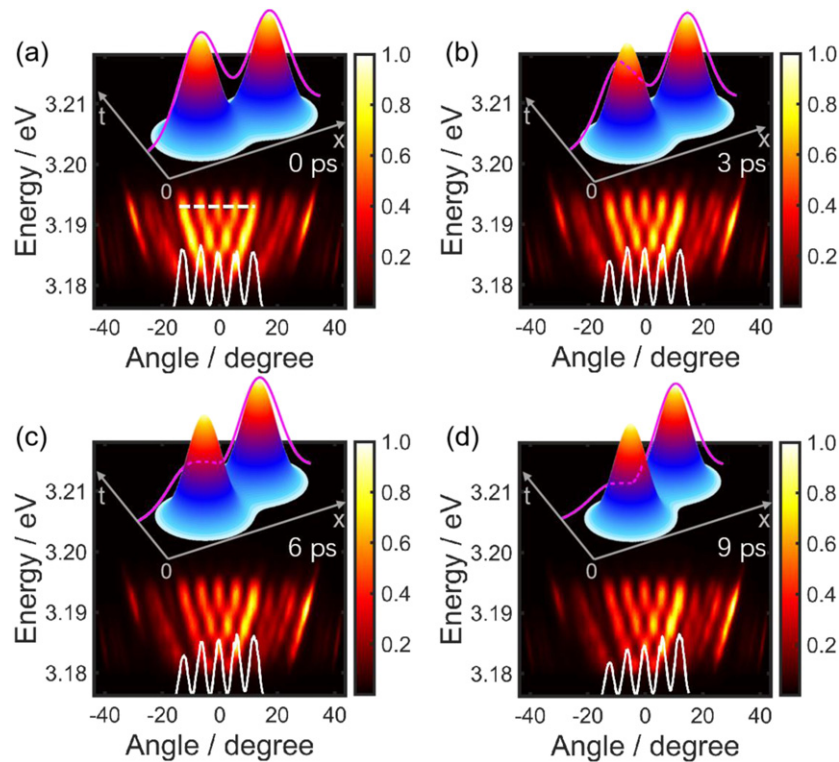


Figure 4. The static PL distributions and the dynamics of polaritons in manipulated potential wells by tuning the delay time of the two excitation laser pulses. The colourful wavepackets represent the distribution of exciton reservoirs in the time and space domain. The magenta lines represent the transient landscapes of the potential wells in real space. The time delays for two laser pulses are (a) 0 ps, (b) 3 ps, (c) 6 ps and (d) 9 ps, respectively. The spatial separation of the two beams is about $5.1 \mu\text{m}$. The white solid lines represent integrated signal at the energy of about 3.193 eV (marked with white dash line in (a)).

in the time-integrated and time-resolved 2D distributions of the PL emissions (shown in figure 3(d)) compared to those obtained for the polariton harmonic oscillators. The dynamical process presented in figure 3(e) follows a different scenario compared to that shown in figure 3(b). The signal first appears on the right side where stronger excitation takes place, while the interference stripes appear later at about 8 ps. Generally, a high contrast of the interference stripes requires comparable population of the two coherent polariton wave packets. Based on this, the observed contrast of the interference pattern can be used to indicate the relative intensity of the polariton wave packets created by two pumping pulses. In the asymmetric excitation case, the polariton populations need a few picoseconds to reach an equivalent level on the two sides, the corresponding dynamics are shown in figures 3(e) and (f). In figure 3(f), the red shift exhibits an extra slow region at the beginning from about 4.5 ps to 9.1 ps (lasting for about 4.6 ps), which can be attributed to that stronger excitation leading to a big polaritonic population, resulting in intense interaction between polaritons which accelerate the process of condensation. Therefore, the polariton condensate first appears in the area of strong excitation. In this case, femtosecond-resolved dynamics in both energy and angle degrees of freedom can be revealed for the polariton harmonic oscillator in a confined potential well at room temperature. The transient potential landscapes and the dynamics can be precisely tailored by the

external optical field, which provides a unique platform for the manipulation of cavity polariton dynamics.

3.3. Dynamics of polariton condensates in temporally manipulated potential wells

In this section, symmetric transient potential wells are realized by tuning the relative delay time of the two exciton pulses, which is realized through a precisely controlled delay line. The anharmonic oscillator dynamics has been realized in these asymmetric potential wells caused by the time delay. Here, it should be noted that the power of the two beams is slightly lower than the condensate threshold. In this case, condensation cannot occur for a single beam excitation. Only when the two laser beams come together can polaritons be sufficiently excited in the ZnO WG microcavity to form new quantum states. The dynamics of the polaritons are driven in the temporally tailored potential wells.

When the femtosecond laser pulse illuminates the ZnO microwire, the exciton reservoir will be generated which performs as a time-dependent potential barrier. Dynamically, part of reservoir excitons couple with cavity photons to produce polaritons. Another exciton reservoir is excited by the second beam which is delayed by a few picoseconds with respect to the first coming beam. The two laser beams can form a time-dependent potential well. The polaritons trapped in the potential well undergo coherent manipulations and quantum harmonic oscillator states can be formed. In our experiment, we

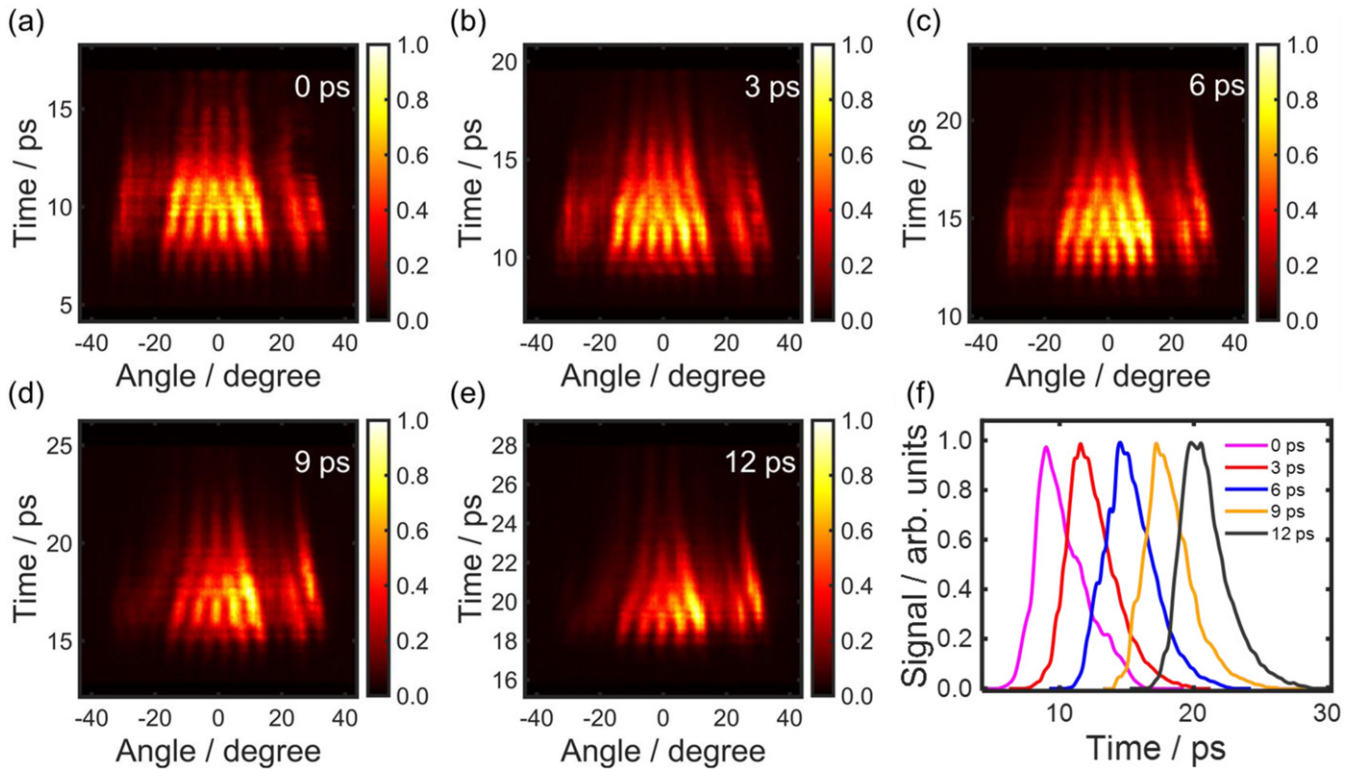


Figure 5. Delay dependent polariton dynamics excited by two beams of femtosecond pulses. (a)–(e) PL distributions as a function of emission angle and time in the momentum space at the delays of 0 ps, 3 ps, 6 ps and 9 ps, respectively, and the corresponding time-resolved signal by projecting the data onto the time axis indicated in (f).

observe the dynamics of the interference patterns of polariton condensates constrained in temporally manipulated potential wells.

As shown in figure 4, two laser beams with equal power are focused on the ZnO microwire at a spatial separation of about $5.1 \mu\text{m}$ to excite polaritons. The second laser pulse illuminating the sample on the right-hand side comes at the delays of 0 ps, 3 ps, 6 ps and 9 ps, respectively. The resulting static angular distributions of the PL emissions are shown in figures 4(a)–(d). As the time delay gets bigger, the signals on the right side become stronger compared to those on the left side, which are clearly shown by the integrated signal of the highest excited state at the bottom of the figures (white lines). Each femtosecond excitation ignites a dynamical exciton reservoir. When the two laser pulses come at different instances, a transient potential well can be produced which undergo distinct development, as illustrated in the inserted figures in figures 4(a)–(d).

Varying the time delay can produce transient asymmetric potential wells, therefore resulting in polariton anharmonic oscillators. These can be clearly visualized in the time-resolved angular distributions of the PL emission shown in figures 5(a)–(e). In these figures, we can see that the asymmetry of the signal strength on the right side with respect to that on the left side is getting bigger as the delay becomes larger. In addition, when we increase the time delay between the two pumping pulses, the dynamics of the overall polariton yields can be manipulated, the distribution of polariton population

can be illustrated by projecting the signals in figures 5(a)–(e) onto the time axis, which is shown in figure 5(f). We found that the maximum population will shift with the time delay. In this set of experiments, the first beam cannot create significant polariton condensates without the participation of the second beam. Only after the second beam arrives at a certain delay, the transient potential barrier created by two beams makes the polaritons being constrained and occupying the harmonic oscillator states. The whole dynamical behavior of the constrained polaritons is determined by the instantaneous potential landscapes formed by the two delayed laser pulses.

3.4. Theoretical modeling

The dynamics of the polariton harmonic/anharmonic oscillator are simulated using the Gross–Pitaevskii equation [32–34]. Due to the ultrafast injection, the potential barrier caused by the optical field disappears in hundreds of femtoseconds. The potential formed by the induced exciton reservoir possesses a longer lifetime thus dominates the polariton harmonic oscillator formation and relaxation. In addition, hot excitons created by nonresonant excitation and reservoir excitons relaxed from hot excitons contribute to the generation of potential wells.

The equations are written as follows.

$$\frac{\partial n_p}{\partial t} = P(x, t) - \gamma_p n_p - m_p n_R \quad (1)$$

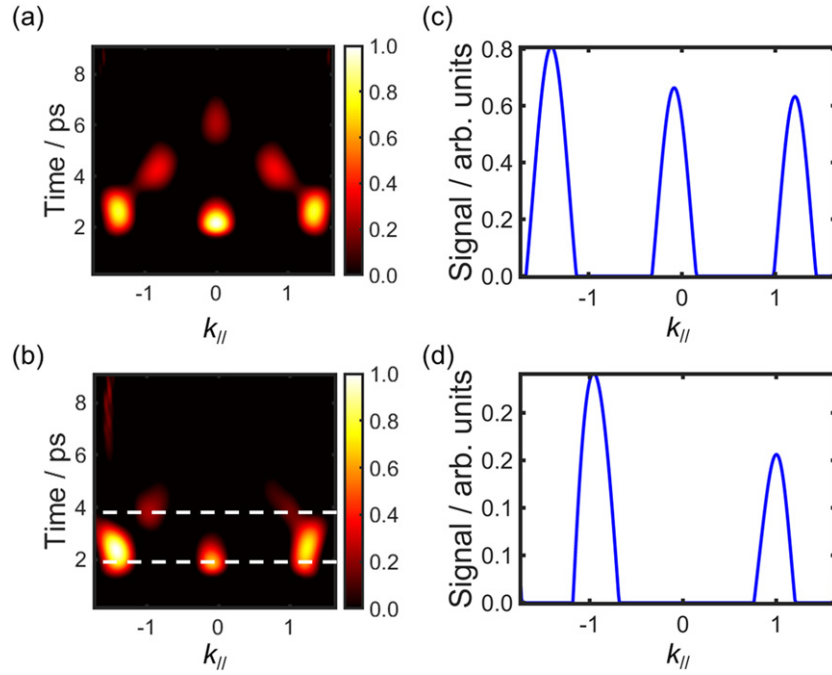


Figure 6. Simulated results using the Gross–Pitaevskii equation. The time-resolved angular distributions of the PL emission for the (a) harmonic and (b) anharmonic oscillators. (c) and (d) present the integrated angular distributions of polaritons for two different delay times, e.g. at 2 ps, and 4 ps, obtained from the data of shown in figure 6(b).

$$\frac{\partial n_R}{\partial t} = n_p n_R - R n_R |\psi|^2 - \gamma_R n_R \quad (2)$$

$$i \frac{\partial \psi}{\partial t} = \left[-\frac{\hbar}{2m^*} \nabla^2 + g_R n_R + g_p n_p + g_c |\psi|^2 \right] \psi + i(R n_R - \gamma_c) \psi. \quad (3)$$

Here $P(x, t)$ is the pump power. ψ represents polariton wavefunction. $n_p(n_R)$ and $\gamma_p(\gamma_R)$ represent the density and the decay rate of the hot excitons (reservoir excitons), respectively. r represents the energy relaxation rate of the hot excitons into the reservoir excitons. g_p , g_R and g_c represent the contact interaction strength. m^* is the effective mass of polariton. R stands for the scattering rate from the exciton reservoir to the lower polariton branch. The simulated result showing polariton harmonic oscillator state transiting from three nodes to two and eventually towards one node is presented in figure 6. The strength of the signal gradually decays as time going. These phenomena agree qualitatively with the experimental observations for polariton harmonic oscillators shown in figures 2 and 3.

4. Conclusions

In summary, we have visualized the femtosecond dynamics of confined polariton wave packets in tailored potential wells at room temperature using the FARSI technique. The landscape of the potential wells are tailored in space by tuning the relative excitation power of the two pumping beams and their spatial separation. Temporal manipulation of the instantaneous potential well is realized by precisely control the relative time

delay between the two excitation pulses. The dynamics of the polaritons confined in the tailored potential wells are explicitly visualized in momentum and energy degrees of freedom. The polariton tends to form quantum harmonic oscillators in a highly excited state initially and follows picosecond relaxations. The interference pattern follows a general tendency that the nodes initially formed at high state preferentially combine and generate a new one at the low state within small emission angles, while the nodes in larger angles shift towards smaller angles. In energy domain, the polaritons undergo redshifts due to the inter-quasiparticle interactions. The experimental clarification of these dynamics and the related mechanisms can definitely improve the development of polariton-based physics and devices. Our femtosecond-resolved measurement technique can serve as a powerful tool for further investigations of ultrafast dynamics. By exploiting advanced microstructure engineering [35] and light field manipulation, complex potential landscapes can be created for manipulating the dynamics of cavity polaritons.

Acknowledgments

We thank Dr Z Wang for the fruitful discussions. This work is supported by the National Key R & D Program of China (Grant Nos. 2018YFA0306303, 2018YFA0306304); the National Natural Science Fund (Grants No. 92050105, 91950201, 11834004, 11621404, 11704124, 11674069 and 11574205); the project supported by the Shanghai Committee of Science and Technology, China (Grant No. 19ZR1473900); Shanghai Municipal Science and Technology Major Project.


Conflict of interest

We have no conflict of interest for this work to be declared.

Data availability statement

The data that support the findings of this study are available from the corresponding author upon reasonable request.

ORCID iDs

Fei Chen  <https://orcid.org/0000-0001-6239-0225>
 Fenghao Sun  <https://orcid.org/0000-0003-0210-5204>
 Huailiang Xu  <https://orcid.org/0000-0001-8469-7041>
 Jian Wu  <https://orcid.org/0000-0002-1318-2291>

References

- [1] Kavokin A and Malpuech G 2003 *Cavity Polaritons* (Amsterdam: Elsevier)
- [2] Hopfield J J 1958 *Phys. Rev.* **112** 1555
- [3] Byrnes T, Kim N Y and Yamamoto Y 2014 *Nat. Phys.* **10** 803–13
- [4] Dang L S, Heger D, André R, Bœuf F and Romestain R 1998 *Phys. Rev. Lett.* **81** 3920
- [5] Deng H, Weihs G, Santori C, Bloch J and Yamamoto Y 2002 *Science* **298** 199–202
- [6] Deng H, Weihs G, Snoke D, Bloch J and Yamamoto Y 2003 *Proc. Natl Acad. Sci.* **100** 15318–23
- [7] Kasprzak J *et al* 2006 *Nature* **443** 409–14
- [8] Sanvitto D and Kéna-Cohen S 2016 *Nat. Mater.* **15** 1061–73
- [9] Ballarini D, De Giorgi M, Cancellieri E, Houdré R, Giacobino E, Cingolani R, Bramati A, Gigli G and Sanvitto D 2013 *Nat. Commun.* **4** 1778
- [10] Zasedatelev A V, Baranikov A V, Urbonas D, Scafirimuto F, Scherf U, Stöferle T, Mahrt R F and Lagoudakis P G 2019 *Nat. Photon.* **13** 378–83
- [11] Balili R, Hartwell V, Snoke D, Pfeiffer L and West K 2007 *Science* **316** 1007–10
- [12] Amo A *et al* 2009 *Nature* **457** 291–5
- [13] Wertz E *et al* 2010 *Nat. Phys.* **6** 860–4
- [14] Belykh V V and Sob'yanin D N 2014 *Phys. Rev. B* **89** 245312
- [15] Sun L, Chen Z, Ren Q, Yu K, Bai L, Zhou W, Xiong H, Zhu Z Q and Shen X 2008 *Phys. Rev. Lett.* **100** 156403
- [16] Xie W, Dong H, Zhang S, Sun L, Zhou W, Ling Y, Lu J, Shen X and Chen Z 2012 *Phys. Rev. Lett.* **108** 166401
- [17] Chen F *et al* 2021 arXiv:2105.08302
- [18] Luo S, Liao L M, Zhang Z, Wang J, Shen X C and Chen Z H 2020 *Phys. Rev. Appl.* **13** 044052
- [19] Xu C, Zhou B, Wang X, Tian C, Zhang Y, Dong H, Wang G and Zhou W 2019 *Opt. Express* **27** 24938
- [20] Zhang X, Zhang Y, Dong H, Tang B, Li D, Tian C, Xu C and Zhou W 2019 *Nanoscale* **11** 4496
- [21] Tosi G, Christmann G, Berloff N G, Tsotsis P, Gao T, Hatzopoulos Z, Savvidis P G and Baumberg J J 2012 *Nat. Phys.* **8** 190–4
- [22] Song H G, Choi S, Park C H, Gong S-H, Lee C, Kwon M S, Choi D G, Woo K Y and Cho Y-H 2019 *Optica* **6** 1313–20
- [23] Zhang X, Zhang Y, Tang B, Tian C, Xu C, Dong H and Zhou W 2019 *Appl. Phys. Express* **12** 012001
- [24] Zhang L *et al* 2015 *Proc. Natl Acad. Sci. USA* **112** E1516–9
- [25] Tanese D *et al* 2013 *Nat. Commun.* **4** 1749
- [26] Dominici L *et al* 2015 *Nat. Commun.* **6** 8993
- [27] Appavoo K, Sfeir M Y and Sfeir M Y 2014 *Rev. Sci. Instrum.* **85** 055114
- [28] Arzhantsev S and Maroncelli M 2005 *Appl. Spectrosc.* **59** 206–20
- [29] Wang J *et al* 2015 *Phys. Rev. B* **91** 165423
- [30] Askitopoulos A, Liew T C H, Ohadi H, Hatzopoulos Z, Savvidis P G and Lagoudakis P G 2015 *Phys. Rev. B* **92** 035305
- [31] Liew T C H, Rubo Y G, Sheremet A S, Liberato S D, Shelykh I A, Laussy F P and Kavokin A V 2016 *New J. Phys.* **18** 023041
- [32] Wouters M, Liew T C H and Savona V 2010 *Phys. Rev. B* **82** 245315
- [33] Wouters M and Carusotto I 2007 *Phys. Rev. Lett.* **99** 140402
- [34] Keeling J and Berloff N G 2008 *Phys. Rev. Lett.* **100** 250401
- [35] Sala V G *et al* 2015 *Phys. Rev. X* **5** 011034